Applied Physics Letters ARTICLE scitation.org/journal/apl

Atomic-resolution *in-situ* cooling study of oxygen vacancy ordering in $La_{0.5}Sr_{0.5}CoO_{3-\delta}$ thin films

Cite as: Appl. Phys. Lett. **114**, 233101 (2019); doi: 10.1063/1.5098886
Submitted: 4 April 2019 · Accepted: 20 May 2019 ·
Published Online: 10 June 2019

Xue Rui[a] and Robert F. Klie

AFFILIATIONS

Department of Physics, University of Illinois at Chicago, Chicago, Illinois 60607, USA

[a]Author to whom correspondence should be addressed: xrui3@uic.edu

ABSTRACT

The presence and potential ordering of oxygen vacancies play an important role in determining the electronic, ionic, and thermal transport properties of many transition metal oxide materials. Controlling the concentration of oxygen vacancies, as well as the structures of ordered oxygen vacancy domains, has been the subject of many experimental and theoretical studies. In epitaxial thin films, the concentration of oxygen vacancies and the type of ordering depend on the structure of the substrate as well as the lattice mismatch between the thin films and the substrate. However, the role of temperature or structural phase transitions in either the substrate or the epitaxial thin films in the oxygen vacancy ordering has remained largely unexplored. In particular, atomic-resolution imaging and spectroscopy analysis of oxygen vacancy ordering in thin films at temperatures below 300 K have not yet been reported. Here, we use aberration-corrected scanning transmission electron microscopy combined with *in-situ* cooling experiments to characterize the atomic/electronic structures of oxygen-deficient $La_{0.5}Sr_{0.5}CoO_{3-\delta}$ thin films grown on $SrTiO_3$ across its antiferrodistortive phase transition at 105 K. We demonstrate that atomic-resolution imaging and electron energy-loss spectroscopy can be used to examine variations in the local density of states as a function of sample temperature.

Functional transition metal oxides have attracted a great deal of experimental and theoretical interest due to their wide range of properties, suitable for numerous practical applications, including fuel-cells,[1] catalysts,[2] thermoelectrics,[3] spintronics,[4] and nanoelectronics.[5] Perovskite oxides of the form ABO_3 (B = Mn, Cr, Ti, Fe, Ni, Co) present a particularly interesting group of functional transition metal oxides, where the interplay of four degrees of freedom, lattice, orbital, charge, and spin generate a complex variety of ground states.[6,7] An important attribute of this class of materials is that no single interaction or degree of freedom dominates.[8] Consequently, subtle changes in external and internal parameters, such as temperature, electric or magnetic fields, strain at interfaces or defects, or ionic radii due to dopants, may tremendously affect the overall properties of the system.[9–12] Fascinating transport properties, such as high-temperature superconductivity[13,14] and thermoelectric,[15,16] ferro-electric,[17,18] proton-,[19,20] or magnetotransport,[21,22] are related to such induced phase transitions between different ground states and types of ordering.

It has become increasingly clear that oxygen vacancy ordering plays an important role in controlling multiple physical properties, such as ferroelectric,[23,24] electronic,[25] ionic,[26] or thermal transport[27] as well as magnetic properties.[28] In transition metal perovskite oxides, oxygen vacancies can form ordered structures, such as the brownmillerite (BM) structure, where vacancies order in alternating planes along the *c*-axis forming fully stoichiometric oxygen octahedral and oxygen deficient tetrahedral layers.[29] This ordering of vacancies does not only give rise to charge disproportionation of the transition metal ions on the *B* site but also cause periodic changes in the perovskite lattice constant.[30] The competition between the interlayer separation between tetrahedral planes and tetrahedral chain distortion within the tetrahedral plane results in diversities of BM domains of different symmetries.[31] Furthermore, this ordered oxygen vacancy can also interact with the ferroelastic distortions, lowering the lattice stability and inducing the polar behavior within a given heterostructure.[32,33]

Oxygen vacancy ordering resulting in the formation of BM structures has been reported in oxygen-deficient $SrCoO_{3-\delta}$,[34] Sr-doped $LaCoO_{3-\delta}$ poly-crystalline bulk[35] and thin films,[36–38] as well as other perovskite Co-oxides.[39] In $La_{1-x}Sr_xCoO_{3-\delta}$, where $x > 0.5$, the formation of oxygen vacancies is enabled by the instability of Co^{4+} in octahedral coordination, preferring a conversion to Co^{2+}/Co^{3+} while releasing oxygen.[40] In the thin film form, the lattice mismatch between epitaxial $La_{1-x}Sr_xCoO_{3-\delta}$ thin films and the substrate can result in biaxial strain stress, which will affect the domain orientation of oxygen vacancies in the BM structure. Biaxial strain modulation can be used to control the oxygen vacancy ordering structure, thus modifying the functionality of the thin film.[41,42]

In addition to the interfacial strain modulation of the thin film, coupling of interfacial oxygen octahedral tilts between the substrate

and the thin films can also be used to modify the epitaxial films' electronic/magnetic behavior. This physical property has been demonstrated to directly couple to octahedral rotations since the octahedral tilt angle is associated with the B-O-B bonding angle and the length via the overlap of the *d* orbitals and localized charge carriers.[43] Recent studies have demonstrated that the magnetic properties of $La_{0.5}Sr_{0.5}CoO_3$ thin films are affected by the choice of substrates, such as $NdGaO_3$ and $(LaAlO_3)_{0.3}(Sr_2AlTaO_6)_{0.7}$ (LSAT). While these substrates have nearly the same lattice spacing (3.861 Å for $NdGaO_3$ and 3.868 Å for LSAT), they exhibit different oxygen octahedral tilting patterns ($a^-a^-a^+$ for $NdGaO_3$ and $a^0a^0a^0$ for LSAT), which appear to influence the ferromagnetic ordering in epitaxial thin films.[38]

In this paper, we directly examine the effects of structural phase transitions of the thin film substrate on the oxygen vacancy ordering and electronic structure of epitaxial $La_{0.5}Sr_{0.5}CoO_{3-\delta}$ ($LSCO_{3-\delta}$) thin films. Specifically, $SrTiO_3$ (STO) is known to undergo an antiferrodistortive (AFD) phase transition from the cubic structure to the tetragonal structure at 105 K, which is due to the antiphase rotation of TiO_6 oxygen octahedral around one of the unit cell axes.[44] Due to the improved stability of our *in-situ* cooling stage, we are now able to achieve atomic-resolution scanning transmission electron microscopy (STEM) imaging and column-resolved electron energy-loss (EEL) spectroscopy at cryogenic temperature. Therefore, we combine *in-situ* cooling using LN_2 with atomic-resolution STEM/EELS to characterize the degree of coupling between the rotated TiO_6–CoO_6 at the interface and the vacancy ordering domain of thin film. $LSCO_{3-\delta}$ films grown on $LaAlO_3$ (LAO) substrates are used as a reference sample to distinguish the effects of interfacial strain and the STO structural phase transition at cryogenic temperature (95 K). While atomic-resolution STEM imaging at cryogenic temperature has been previously reported,[45–48] atomic-column resolved EELS has not yet been demonstrated at 95 K.

First, the structure of ordered oxygen vacancy domains is characterized at cryogenic temperature (95 K) and compared with structures found at room temperature using atomic-resolution high angle annular dark field (HAADF) imaging. Figure 1 shows atomic-resolution HAADF STEM images of $La_{0.5}Sr_{0.5}CoO_{3-\delta}$ on $SrTiO_3$ (STO) and $LaAlO_3$ (LAO) substrates in the [1 0 0] orientation at 300 K and 95 K, respectively (initial images are shown in Fig. S1). Since the contrast of HAADF images is directly proportional to the average atomic number of the imaged elements, La/Sr in columns can be seen as the highest intensity contrast in Fig. 1. The most noticeable feature of the $LSCO_{3-\delta}$ film is dark and bright stripes, visible at both room and cryogenic temperatures, which has been previously reported as the brownmillerite structure (BM), where the oxygen vacancies order in alternating oxygen octahedral and tetrahedral planes along the (001) direction.[36,49] This superlattice feature appears perpendicular to the interface in $LSCO_{3-\delta}$ films on STO, while ordering parallel to the interface is observed in $LSCO_{3-\delta}$ films grown on the LAO substrate. This is similar to what Gazquez *et al.* reported, where the −1.2% mismatch between $LaAlO_3$ (3.789 Å) and bulk $La_{0.5}Sr_{0.5}CoO_3$ (3.836 Å) enables oxygen vacancy ordering parallel to the interface, while the 1.8% mismatch between $SrTiO_3$ (3.905 Å) and $La_{0.5}Sr_{0.5}CoO_3$ results in tensile strain of the films, enabling oxygen vacancy ordering perpendicular to the interface.[50] Furthermore, it can be seen that the dark and bright columns do not directly touch the substrate/film interface. We suggest that this is due to the tendency of oxygen vacancies to clustering near the surface instead of the substrate/film interface. As Petrie *et al.*[51] and Tahini *et al.*[52] reported for in-plane biaxial strain effects on the formation of oxygen vacancies in the $SrCoO_{3-\delta}$, the tensile strain at the surface lowers the oxygen vacancy formation energy and facilitates the oxygen vacancy ordering to form near the surface. In addition, the epitaxial lattice spacing of $LSCO_{3-\delta}$ results in a strained thin film that forces the oxygen vacancy to disorder at the $LSCO_{3-\delta}$/STO interface.[53] It appears that the critical length scale for such an effect is 4–5 unit cells.

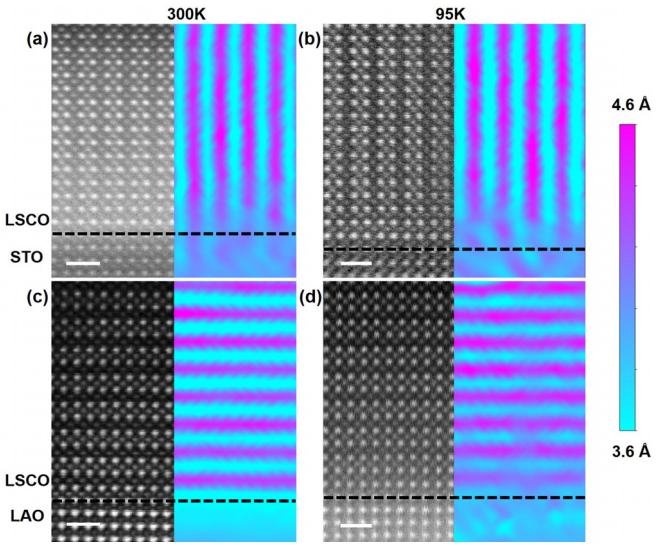

FIG. 1. (a) and (b) Left part shows the representative HAADF image of the $LSCO_{3-\delta}$ thin film grown on the STO substrate at 300 K and 95 K. Right part shows the La-La interatomic spacing colormaps for left images. (c) and (d) Left part shows the Representative atomic-resolution HAADF image of the $LSCO_{3-\delta}$ thin film grown on the LAO substrate at 300 K and 95 K, respectively. The right section of the image represents the interatomic spacing colormap.

To quantify the effects of sample temperature on the BM lattice parameters, the La/Sr interatomic distances in the bright and dark layers were measured in $LSCO_{3-\delta}$ films using HAADF images similar to those shown in Fig. 1. Representative maps of the La/Sr-site interatomic spacing are also shown in Fig. 1. In $LSCO_{3-\delta}$ films grown on STO, we find that the in-plane La/Sr interatomic spacing at room temperature is 3.63 Å for the bright layers and 4.29 Å for the dark layers, as previously reported by Gazquez *et al.*[50] After cooling down to 95 K, the La/Sr spacing in the bright layers decreases by 0.1 Å, while in the dark layers, it is increased by 0.04 Å. We do not find any measurable change in the La/Sr interatomic distances in the out-of-plane direction as a function of sample temperature.

For $LSCO_{3-\delta}$ films grown on LAO, the La/Sr-La/Sr interatomic distances in both the in-plane direction and the out-of-plane direction are not affected by the sample cooling to 95 K. A summary of the statistical average interatomic distances for both kinds of samples is given in Table S1. The fact that the La/Sr interatomic distances are dependent on the sample temperature only in films grown on STO suggests that the substrate's phase transition has an effect on the oxygen vacancy ordering in the $LSCO_{3-\delta}$ film.

In addition to the BM-type structure of oxygen vacancy ordering, many other forms of ordered vacancies have been suggested in $LSCO_{3-\delta}$.[54] Therefore, we use the annular bright field (ABF) image,

which is sensitive to light elements such as oxygen, to directly image the oxygen coordinate environment in the $LSCO_{3-\delta}$ thin films. The pseudo cubic [1 1 0] or [1 −1 0] projections provide the best viewing direction to establish the oxygen vacancy ordering type since the oxygen atomic columns are clearly visible as shown in Figs. 2(a) and 2(b). For the $LSCO_{3-\delta}$ film on STO, we focus on an area where the oxygen vacancy ordering domain is parallel to the interface and image the oxygen vacancy ordering in the [1 1 0] direction. Figure 2(a) shows the $LSCO_{3-\delta}$ film on STO, where the shift of the Co atomic columns as a result of missing oxygen columns is clearly visible. The proposed structure for the BM phase is shown in [0 1 0], which agrees with the structure observed in Fig. 2(a). An ABF image of $LSCO_{3-\delta}$ on LAO in the [1 −1 0] direction is shown in Fig. 2(b), where no shift in the Co column but the columns with oxygen vacancies are clearly visible. This structure matched the BM phase in the [1 0 0] orientation. Therefore, oxygen deficient $LSCO_{3-\delta}$ films grown on either STO or LAO exhibit the BM-type oxygen vacancy ordering phase.

In the [1 0 0] projection, shown in the ABF image in Fig. 2(c), the BM phase of the $LSCO_{3-\delta}$ thin film appears to be distorted, potentially due to the in-plane strain imposed by the STO substrate. Compared to the standard BM structure in the same orientation, the oxygen atoms in the tetragonal CoO_4 column and the adjacent octahedral CoO_6 columns are shifted as indicated in Fig. 2(c). The $LSCO_{3-\delta}$ films on LAO show the expected BM structure, as seen in Fig. 2(d).

The electronic structure for the $LSCO_{3-\delta}$/STO heterostructure is examined as a function of temperature using EELS. The EEL near-edge fine-structure (ELNES) has been widely applied to characterize the 3*d* orbital configuration and valence state in transition metal oxides. In this paper, spectra of the O *K*-edge and Ti *L*-edge are first acquired from the $SrTiO_3$ substrate at both room and cryogenic

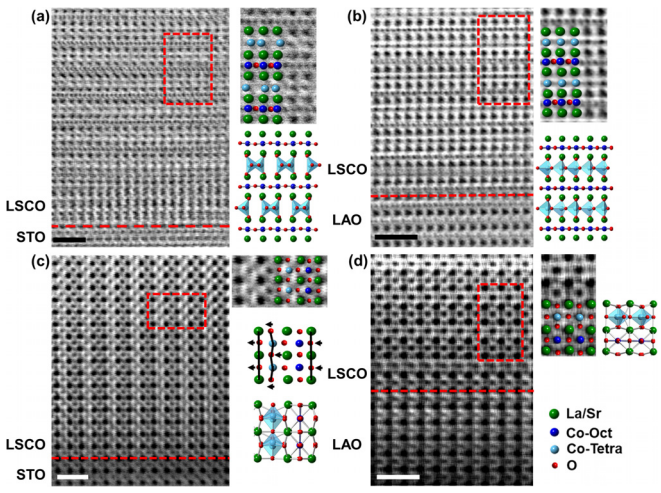

FIG. 2. (a) ABF image of the $LSCO_{3-\delta}$thin film grown on the STO substrate along [1 1 0]. The marked area shows the same structure as the standard BM structure in the [0 1 0] direction. (b) ABF image of the $LSCO_{3-\delta}$ thin film grown on the LAO substrate along [1 −1 0], and the marked area shows the same structure as the standard BM structure in the [1 0 0] direction. (c) ABF image of the $LSCO_{3-\delta}$ thin film grown on the STO substrate along [1 0 0]. The arrows mark the shift of the oxygen atom compared to the standard BM-structure. (d) ABF image of the $LSCO_{3-\delta}$ thin film grown on the LAO substrate along [1 0 0], and the marked area shows the same structure as the standard BM-structure. The scale bar is 1 nm.

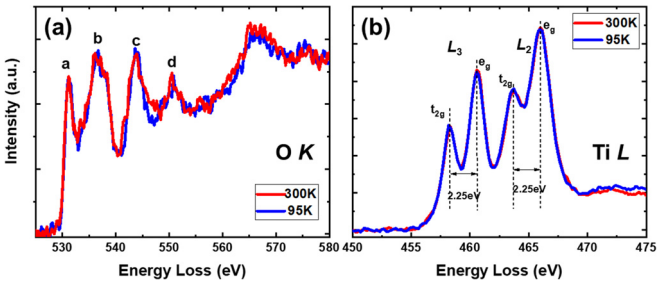

FIG. 3. (a) O *K*-edge acquired on the $SrTiO_3$ substrate at room temperature and cryogenic temperature. (b) Ti *L*-edge acquired on the $SrTiO_3$ substrate at room temperature and cryogenic temperature.

temperatures to probe the effects of the STO phase transition on the ELNES. As shown in Fig. 3(a), both O *K*-edge spectra at 300 K and 95 K exhibit four prominent peaks, marked as *a*, *b*, *c*, and *d*. The intensity of peak *a* has been associated with the hybridization of the O 2*p* and Ti 3*d* orbitals,[55] providing information of the Ti 3*d* t_{2g} and e_g orbital occupancy.[56] However, we find that there is no change in the O *K*-edge of $SrTiO_3$ as a function of temperature. Figure 3(b) shows the Ti *L*-edge spectra at 300 K and 95 K. Here, four peaks can be seen due to the splitting of Ti 3*d* final states into the t_{2g} and e_g orbitals, as well as the initial Ti $2p^{3/2}$ and $2p^{1/2}$ states.[57] Similar to the O *K*-edge ELNES, we do not find any change in the Ti *L*-edges of $SrTiO_3$ as a function of sample temperature. We proposed that core-loss EELS is not sensitive enough or it does not provide a sufficient energy resolution to observe the changes in the electronic structure as a result of the STO phase transition at 105 K.

Using the *in-situ* cooling EELS analysis in the $LSCO_{3-\delta}$ thin film, shown in Fig. S2, we can detect the change in the Co 3d electronic configuration in oxygen vacancy ordering regions associated with the STO substrate phase transition as a function of temperature. To determine the Co 3d orbital occupancy in the dark and bright layers of the $LSCO_{3-\delta}$ thin films independently, atomic-column resolved EELS was acquired at 300 K and 95 K. Figure 4(a) shows the O *K*-edge for bright and dark layers in the $LSCO_{3-\delta}$ film on STO at 95 K. The O *K*-edge prepeak for the bright layers is located at 526 eV and at 527 eV in the dark layers. The Co *L*-edge spectra taken at 95 K are shown in Fig. 4(b). We determine that the Co white line ratio for bright layers is 3.0, while it is 3.8 in the dark layers. Using the relationship between the Co white line ratio and the Co valence state,[58] we find that the valence state for the bright layer is Co 2.9+ and Co 2.5+ for the dark layers.

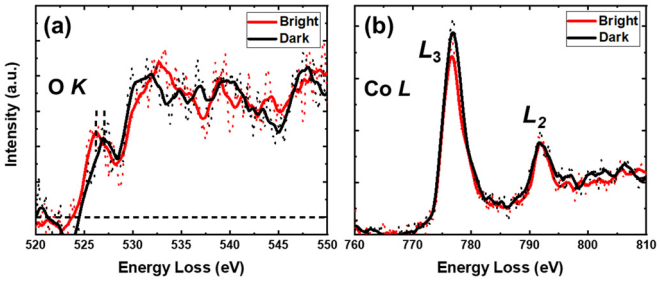

FIG. 4. (a) and (b) O *K*-edge and Co *L*-edge spectra extracted from dark and bright layers on $LSCO_{3-\delta}$ grown on the STO substrate at cryogenic temperature.

This demonstrates that atomic-column resolved EELS is possible at cryogenic temperature and can distinguish the Co valence state in the different layers of the BM-type oxygen-vacancy ordering. Atomic-column resolved EELS results at 95 K for the $LSCO_{3-\delta}$ thin film on the LAO substrate are shown in supplementary material Fig. S3. Co *L*-edge spectra from $LSCO_{3-\delta}$ films on LAO at 95 K are shown in Fig. S3(b). The measured Co white line ratio is 3.0 for bright layers while 3.9 in the dark layers, indicating a Co valence state of 2.9+ in for bright layers and 2.4+ for the dark layer. Both $LSCO_{3-\delta}$ films on STO and LAO exhibit charge ordering in the oxygen vacancy ordering area, which is similar to the Co valence state between dark and bright in the $LaCoO_{3-\delta}$ thin film grown on the $SrTiO_3$ substrate.[36]

Next, we compare EEL spectra acquired from $LSCO_{3-\delta}$ films on STO at 300 K and 95 K, as shown in Fig. 5. Figure 5(a) shows that the O *K*-edge prepeak at 526 eV in the bright layers is suppressed at room temperature compared to cryogenic temperatures, while the intensity of the prepeak at 527 eV in the dark layers is largely suppressed at room temperature. In Fig. 5(b), the Co *L*-edge appears to be mostly unchanged in both the bright and dark layers as a function of temperature, which demonstrates that the Co valence state/oxygen stoichiometry does not change significantly upon sample cooling. The reference data from $LSCO_{3-\delta}$ films grown on the LAO substrate are shown in Fig. S4. Here, the O *K*-edge and Co *L*-edges remain unchanged in both the dark and bright layers at 300 K and 95 K. This comparison between the same thin film grown on different substrates further suggests that the variation found in the O K-edge prepeak of the $LSCO_{3-\delta}$/STO system is associated with changes in the STO substrate coupling into the $LSCO_{3-\delta}$ layer rather than intrinsic changes in the $LSCO_{3-\delta}$ structure due to sample cooling.

Oxygen vacancy ordering in $La_{0.5}Sr_{0.5}CoO_{3-\delta}$ thin films on the $SrTiO_3$ substrate has previously been studied by Gazquez *et al.*[59] who reported that, using atomic-resolution STEM/EELS and density functional theory (DFT) calculations, in addition to the oxygen vacancies, the Co spin state also appears to order in highly oxygen deficient areas of composition $La_{0.5}Sr_{0.5}CoO_{2.25}$ within the $La_{0.5}Sr_{0.5}CoO_{3-\delta}$ thin film. According to the approximate linear relationship between lattice spacing and oxygen deficiency, δ, proposed by Kim *et al.*,[38] we have determine δ in the area where we performed our STEM/EELS analysis and found that the composition of our films ranges from $La_{0.5}Sr_{0.5}CoO_{2.7}$ to $La_{0.5}Sr_{0.5}CoO_{2.5}$, in good agreement with our average Co valence determination ranging from 2.9+ to 2.5+. We can, therefore, exclude Co spin state ordering at low temperature as the origin of the observed changes in the O K-edge fine-structure. Thus, we propose that the change in the O coordination in the octahedral and tetrahedral structure can explain the difference in the position of the oxygen K-edge prepeak between the bright and dark layers in the BM structure. This is in agreement with the difference in energy levels of the Co 3*d* orbitals in CoO_4 and CoO_6, as discussed by Choi *et al.*[60]

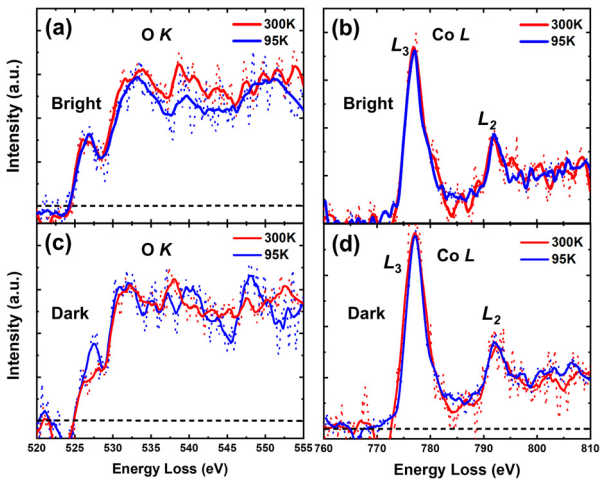

FIG. 5. (a) and (b) O *K*-edge and Co *L*-edge acquired at 300 K and 95 K from the bright layer in $LSCO_{3-\delta}$ on STO. (c) and (d) O K-edge and Co *L*-edge acquired at 300 K and 95 K from the dark layer in $LSCO_{3-\delta}$ on STO.

The extent to which the interfacial coupling influences the physical property of the heterostructure depends on the rigidity of the thin film.[61] It has been demonstrated that CoO_6 exhibit weaker Jahn-Teller distortions compared to MnO_6 in the $La_xSr_{1-x}MnO_3$ thin film by Sundaram *et al.*,[62] which enables CoO_6 to be more easily tilted by TiO_6 octahedral rotation and to maintain the tilted pattern up to 10 nm from the interfaces, compared to only several unit cells in $La_xSr_{1-x}MnO_3$. However, the tensile strain imposed by the STO substrate makes the $LSCO_{3-\delta}$ average lattice spacing remain constant and the observed increase in lattice spacing of the oxygen deficient dark layers of the BM structure leads to a compensating decrease in the interatomic distance of the bright layer. Furthermore, the twin domains that form as a result of the phase rotation of the TiO_6 octahedra during the STO phase transition, as well as the different ligand fields between the CoO_6 octahedra and the CoO_4 tetrahedra, make it possible for the bright and dark layers to respond differently at low temperatures.[30,31] Finally, we have previously reported that the O *K*-edge prepeak is sensitive to Co $3d^6$ spin state transition in $LaCoO_3$.[45] However, in the $LSCO_{3-\delta}$ films reported here, we do not expect a similar Co spin state transition and the mixed Co 2+/3+ valence state makes the determination of the Co ion spin state more difficult compared to $LaCoO_3$. Thus, additional DFT modeling will be required to distinguish the effects of valence and spin state transition in $LSCO_{3-\delta}$ as a function of temperature.

In summary, we have demonstrated that atomic-resolution STEM-EELS analysis can be performed at both room temperature and cryogenic temperature. We have used this approach to directly measure the effects of the STO low temperature antiferrodistortive phase transition on the atomic/electronic structures of oxygen vacancy ordering in $LSCO_{3-\delta}$ thin films. We find that both the lattice spacing and the O *K*-edge fine structures in dark and bright layers of the BM-type oxygen vacancy ordered domains respond in different ways during the cooling experiment, only in films grown on STO. The same films grown on LAO do not show any temperature dependent changes in the atomic and electronic structures. Similar experimental approaches to atomic-resolution STEM imaging and EELS can now be used to explore structural transition in a large range of function transition metal oxide materials as a function of temperature.

See the supplementary material for representative HAADF images acquired during *in-situ* cooling experiment, table for statistic lattice measurements, *in-situ* cooling EELS data for the $LSCO_{3-\delta}$ thin film grown on STO and LAO, and reference *in-situ* cooling atomic-column resolved EELS data for $LSCO_{3-\delta}$ on LAO.

The authors want to thank Jeff Walter and Chris Leighton (University of Minnesota) for growing $La_{0.5}Sr_{0.5}CoO_{3-\delta}$ thin film

samples. This work was supported by a grant from the National Science Foundation (Grant No. DMR-1831406). The acquisition of the UIC JEOL JEM-ARM200CF was supported by the NSF MRI-R^2 grant (No. DMR-0959470), and the acquisition of the Gatan Continuum spectrometer was supported by a grant from the National Science foundation MRI Program (No. DMR-1626065). Support from the UIC Research Resources Center (RRC), in particular A. W. Nicholls and F. Shi, is acknowledged.

REFERENCES

[1]S. B. Adler, Chem. Rev. **104**(10), 4791 (2004).
[2]J. Haber, in *Solid State Chemistry in Catalysis* (American Chemical Society, 1985), pp. 3.
[3]S. Walia, S. Balendhran, H. Nili, S. Zhuiykov, G. Rosengarten, Q. H. Wang, M. Bhaskaran, S. Sriram, M. S. Strano, and K. Kalantar-zadeh, Prog. Mater. Sci. **58**(8), 1443 (2013).
[4]S. A. Wolf, D. D. Awschalom, R. A. Buhrman, J. M. Daughton, S. von Molnár, M. L. Roukes, A. Y. Chtchelkanova, and D. M. Treger, Science **294**(5546), 1488 (2001).
[5]P. Poizot, S. Laruelle, S. Grugeon, L. Dupont, and J. M. Tarascon, Nature **407**, 496 (2000).
[6]S. V. Kalinin, A. Borisevich, and D. Fong, ACS Nano **6**(12), 10423 (2012).
[7]H. Y. Hwang, Y. Iwasa, M. Kawasaki, B. Keimer, N. Nagaosa, and Y. Tokura, Nat. Mater. **11**, 103 (2012).
[8]M. A. Peña and J. L. G. Fierro, Chem. Rev. **101**(7), 1981 (2001).
[9]M. A. Señarís-Rodríguez and J. B. Goodenough, J. Solid State Chem. **116**(2), 224 (1995).
[10]P. M. Raccah and J. B. Goodenough, J. Appl. Phys. **39**(2), 1209 (1968).
[11]J. M. Rondinelli and N. A. Spaldin, Phys. Rev. B **81**(8), 085109 (2010).
[12]P. Gao, J. Britson, C. T. Nelson, J. R. Jokisaari, C. Duan, M. Trassin, S. H. Baek, H. Guo, L. Li, Y. Wang, Y. H. Chu, A. M. Minor, C. B. Eom, R. Ramesh, L. Q. Chen, and X. Pan, Nat. Commun. **5**, 3801 (2014).
[13]Y. Maeno, H. Hashimoto, K. Yoshida, S. Nishizaki, T. Fujita, J. G. Bednorz, and F. Lichtenberg, Nature **372**(6506), 532 (1994).
[14]K. A. Muller, M. Takashige, and J. G. Bednorz, Phys. Rev. Lett. **58**(11), 1143 (1987).
[15]I. Terasaki, Y. Sasago, and K. Uchinokura, Phys. Rev. B **56**(20), 12685 (1997).
[16]M. Jaime, M. B. Salamon, M. Rubinstein, R. E. Treece, J. S. Horwitz, and D. B. Chrisey, Phys. Rev. B **54**(17), 11914 (1996).
[17]J. Junquera and P. Ghosez, Nature **422**(6931), 506 (2003).
[18]F. Kubel and H. Schmid, Acta Crystallogr., Sect. B **46**, 698 (1990).
[19]H. G. Bohn and T. Schober, J. Am. Ceram. Soc. **83**(4), 768 (2000).
[20]N. Q. Minh, J. Am. Ceram. Soc. **76**(3), 563 (1993).
[21]S. Jin, T. H. Tiefel, M. McCormack, R. A. Fastnacht, R. Ramesh, and L. H. Chen, Science **264**(5157), 413 (1994).
[22]H. Y. Hwang, S. W. Cheong, N. P. Ong, and B. Batlogg, Phys. Rev. Lett. **77**(10), 2041 (1996).
[23]R. V. Wang, D. D. Fong, F. Jiang, M. J. Highland, P. H. Fuoss, C. Thompson, A. M. Kolpak, J. A. Eastman, S. K. Streiffer, A. M. Rappe, and G. B. Stephenson, Phys. Rev. Lett. **102**(4), 047601 (2009).
[24]L. Yao, S. Inkinen, and S. van Dijken, Nat. Commun. **8**, 14544 (2017).
[25]H. Jeen, W. S. Choi, M. D. Biegalski, C. M. Folkman, I. C. Tung, D. D. Fong, J. W. Freeland, D. Shin, H. Ohta, M. F. Chisholm, and H. N. Lee, Nat. Mater. **12**(11), 1057 (2013).
[26]S. Stolen, E. Bakken, and C. E. Mohn, Phys. Chem. Chem. Phys. **8**(4), 429 (2006).
[27]X. Wu, J. Walter, T. Feng, J. Zhu, H. Zheng, J. F. Mitchell, N. Biškup, M. Varela, X. Ruan, C. Leighton, and X. Wang, Adv. Funct. Mater. **27**(47), 1704233 (2017).
[28]H. B. Li, N. Lu, Q. Zhang, Y. Wang, D. Feng, T. Chen, S. Yang, Z. Duan, Z. Li, Y. Shi, W. Wang, W. H. Wang, K. Jin, H. Liu, J. Ma, L. Gu, C. Nan, and P. Yu, Nat. Commun. **8**(1), 2156 (2017).
[29]M. T. Anderson, J. T. Vaughey, and K. R. Poeppelmeier, Chem. Mater. **5**(2), 151 (1993).
[30]A. M. Abakumov, A. S. Kalyuzhnaya, M. G. Rozova, E. V. Antipov, J. Hadermann, and G. Van Tendeloo, Solid State Sci. **7**(7), 801 (2005).
[31]T. G. Parsons, H. D'Hondt, J. Hadermann, and M. A. Hayward, Chem. Mater. **21**(22), 5527 (2009).
[32]J. Young, E. J. Moon, D. Mukherjee, G. Stone, V. Gopalan, N. Alem, S. J. May, and J. M. Rondinelli, J. Am. Chem. Soc. **139**(7), 2833 (2017).
[33]R. Mishra, Y.-M. Kim, J. Salafranca, S. K. Kim, S. H. Chang, A. Bhattacharya, D. D. Fong, S. J. Pennycook, S. T. Pantelides, and A. Y. Borisevich, Nano Lett. **14**(5), 2694 (2014).
[34]S. Stemmer, A. Sane, N. D. Browning, and T. J. Mazanec, Solid State Ionics **130**(1-2), 71 (2000).
[35]A. Gulec and R. F. Klie, J. Appl. Phys. **116**(23), 233701 (2014).
[36]N. Biškup, J. Salafranca, V. Mehta, M. P. Oxley, Y. Suzuki, S. J. Pennycook, S. T. Pantelides, and M. Varela, Phys. Rev. Lett. **112**(8), 087202 (2014).
[37]V. V. Mehta, N. Biskup, C. Jenkins, E. Arenholz, M. Varela, and Y. Suzuki, Phys. Rev. B **91**(14), 144418 (2015).
[38]Y. M. Kim, J. He, M. D. Biegalski, H. Ambaye, V. Lauter, H. M. Christen, S. T. Pantelides, S. J. Pennycook, S. V. Kalinin, and A. Y. Borisevich, Nat. Mater. **11**(10), 888 (2012).
[39]A. Gulec, D. Phelan, C. Leighton, and R. F. Klie, ACS Nano **10**(1), 938 (2016).
[40]G. H. Jonker and J. H. Van Santen, Physica **19**(1), 120 (1953).
[41]C. K. Xie, J. I. Budnick, W. A. Hines, B. O. Wells, and J. C. Woicik, Appl. Phys. Lett. **93**(18), 182507 (2008).
[42]C. Xie, J. I. Budnick, B. O. Wells, and J. C. Woicik, Appl. Phys. Lett. **91**(17), 172509 (2007).
[43]M. D. Biegalski, Y. Takamura, A. Mehta, Z. Gai, S. V. Kalinin, H. Ambaye, V. Lauter, D. Fong, S. T. Pantelides, Y. M. Kim, J. He, A. Borisevich, W. Siemons, and H. M. Christen, Adv. Mater. Interfaces **1**(8), 1400203 (2014).
[44]T. Sakudo and H. Unoki, Phys. Rev. Lett. **26**(14), 851 (1971).
[45]R. F. Klie, J. C. Zheng, Y. Zhu, M. Varela, J. Wu, and C. Leighton, Phys. Rev. Lett. **99**(4), 047203 (2007).
[46]R. Tao, A. Romanenko, L. D. Cooley, and R. F. Klie, J. Appl. Phys. **114**(4), 044306 (2013).
[47]X. Rui, J. Walter, C. Leighton, and R. Klie, Microsc. Microanal. **22**(S3), 1626 (2016).
[48]B. H. Savitzky, I. El Baggari, C. B. Clement, E. Waite, B. H. Goodge, D. J. Baek, J. P. Sheckelton, C. Pasco, H. Nair, N. J. Schreiber, J. Hoffman, A. S. Admasu, J. Kim, S.-W. Cheong, A. Bhattacharya, D. G. Schlom, T. M. McQueen, R. Hovden, and L. F. Kourkoutis, Ultramicroscopy **191**, 56 (2018).
[49]Y. Ito, R. F. Klie, N. D. Browning, and T. J. Mazanec, J. Am. Ceram. Soc. **85**(4), 969 (2002).
[50]J. Gazquez, S. Bose, M. Sharma, M. A. Torija, S. J. Pennycook, C. Leighton, and M. Varela, APL Mater. **1**(1), 012105 (2013).
[51]J. R. Petrie, H. Jeen, S. C. Barron, T. L. Meyer, and H. N. Lee, J. Am. Chem. Soc. **138**(23), 7252 (2016).
[52]H. A. Tahini, X. Tan, U. Schwingenschlögl, and S. C. Smith, ACS Catal. **6**(8), 5565 (2016).
[53]K. Hirai, R. Aso, Y. Ozaki, D. Kan, M. Haruta, N. Ichikawa, H. Kurata, and Y. Shimakawa, ACS Appl. Mater. Interfaces **9**(35), 30143 (2017).
[54]Z. L. Wang and J. S. Yin, Philos. Mag. B **77**(1), 49 (1998).
[55]N. Nakagawa, H. Y. Hwang, and D. A. Muller, Nat. Mater. **5**(3), 204 (2006).
[56]J. C. Woicik, E. L. Shirley, C. S. Hellberg, K. E. Andersen, S. Sambasivan, D. A. Fischer, B. D. Chapman, E. A. Stern, P. Ryan, D. L. Ederer, and H. Li, Phys. Rev. B **75**(14), 30143–30148 (2007).
[57]E. Stoyanov, F. Langenhorst, and G. Steinle-Neumann, Am. Mineral. **92**(4), 577 (2007).
[58]Z. L. Wang, J. S. Yin, and Y. D. Jiang, Micron **31**(5), 571 (2000).
[59]J. Gazquez, W. Luo, M. P. Oxley, M. Prange, M. A. Torija, M. Sharma, C. Leighton, S. T. Pantelides, S. J. Pennycook, and M. Varela, Nano Lett **11**(3), 973 (2011).
[60]W. S. Choi, H. Jeen, J. H. Lee, S. S. Seo, V. R. Cooper, K. M. Rabe, and H. N. Lee, Phys. Rev. Lett. **111**(9), 097401 (2013).
[61]L. Qiao, J. H. Jang, D. J. Singh, Z. Gai, H. Xiao, A. Mehta, R. K. Vasudevan, A. Tselev, Z. Feng, H. Zhou, S. Li, W. Prellier, X. Zu, Z. Liu, A. Borisevich, A. P. Baddorf, and M. D. Biegalski, Nano Lett. **15**(7), 4677 (2015).
[62]N. Sundaram, Y. Jiang, I. E. Anderson, D. P. Belanger, C. H. Booth, F. Bridges, J. F. Mitchell, T. Proffen, and H. Zheng, Phys. Rev. Lett. **102**(2), 026401 (2009).